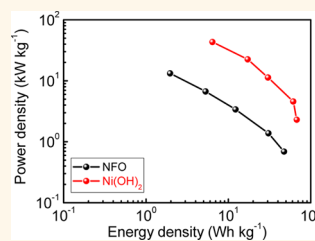# Hydrothermally Formed Three-Dimensional Nanoporous Ni(OH)$_2$ Thin-Film Supercapacitors

Yang Yang,[†,‡] Lei Li,[†] Gedeng Ruan,[†] Huilong Fei,[†] Changsheng Xiang,[†] Xiujun Fan,[†] and James M. Tour*,[†,‡,§]

[†]Department of Chemistry, [‡]Smalley Institute for Nanoscale Science and Technology, and [§]Department of Materials Science and NanoEngineering, Rice University, 6100 Main Street, Houston, Texas 77005, United States

ABSTRACT A three-dimensional nanoporous Ni(OH)$_2$ thin-film was hydrothermally converted from an anodically formed porous layer of nickel fluoride/oxide. The nanoporous Ni(OH)$_2$ thin-films can be used as additive-free electrodes for energy storage. The nanoporous layer delivers a high capacitance of 1765 F g^{-1} under three electrode testing. After assembly with porous activated carbon in asymmetric supercapacitor configurations, the devices deliver superior supercapacitive performances with capacitance of 192 F g^{-1}, energy density of 68 Wh kg^{-1}, and power density of 44 kW kg^{-1}. The wide working potential window (up to 1.6 V in 6 M aq KOH) and stable cyclability (∼90% capacitance retention over 10 000 cycles) make the thin-film ideal for practical supercapacitor devices.

KEYWORDS: nanoporous · nickel hydroxide · hydrothermal treatment · thin-film · supercapacitors

Electrochemical capacitors (ECs) or super-capacitors, including non-Faradaic electric double-layer capacitors (EDLCs, usually composed of carbon materials) based on electrostatic adsorption, and Faradaic pseudocapacitors (such as in transition metal oxides) based on redox reactions, have the advantages of fast dynamic response, high power density, and long-term cyclability. ECs and EDLCs are often used as advanced energy storage devices to bridge the gap between conventional capacitors and rechargeable batteries.[1−3] To expand the potential applications of ECs, the design of new electrode materials having high energy densities without sacrificing power densities is sought.[4] Enhancement of the specific capacitance of the electrode materials or extending the working potential window are two approaches that are based on the mathematical description of energy density, $E = 1/2CU^2$, where U is the operation potential window.[5] Extension of the potential window has been most studied due to its quadratic relationship to the energy density.[6] Organic electrolytes or ionic liquids have been used to replace aqueous electrolytes due to their much wider potential windows (over 2 V) when compared to aqueous electrolytes. Unfortunately, these materials increase the cost of the devices.[7,8] Recently, ECs designed in asymmetric two-electrode configurations by using different electrode materials with unmatched working potential windows have delivered a wider operating voltage up to 1.6 V in aqueous electrolytes.[9] To that end, transition metal (Ni, Mn, Co, etc.) oxides or hydroxides are under consideration to construct asymmetric supercapacitors due to their high theoretical values for the specific capacitance.[10] Among those transition metal oxides and hydroxides, NiO and Ni(OH)$_2$ have been studied due to their natural abundance and low cost which render them as promising candidates to replace the very expensive RuO$_2$.[11,12] In recent years, an approach to enhance the specific capacitance was developed by fabricating hybrid materials from EDLCs (graphene and carbon nanotubes) with Faradaic pseudocapacitors (transition metal oxides or hydroxides) to integrate advantages derived from both materials.[13] The fabrication of nanoporous metal oxides or hydroxides with high surface area is another approach to combine non-Faradaic and Faradaic processes into the same material. This would afford improved capacitor performance because of the greatly increased number of redox reaction sites in the porous structure and fast ion transport through the channels.[2] However, it is a challenge to fabricate three-dimensional (3-D) nanoporous Ni(OH)$_2$ directly on metal substrates to produce components for additive-free
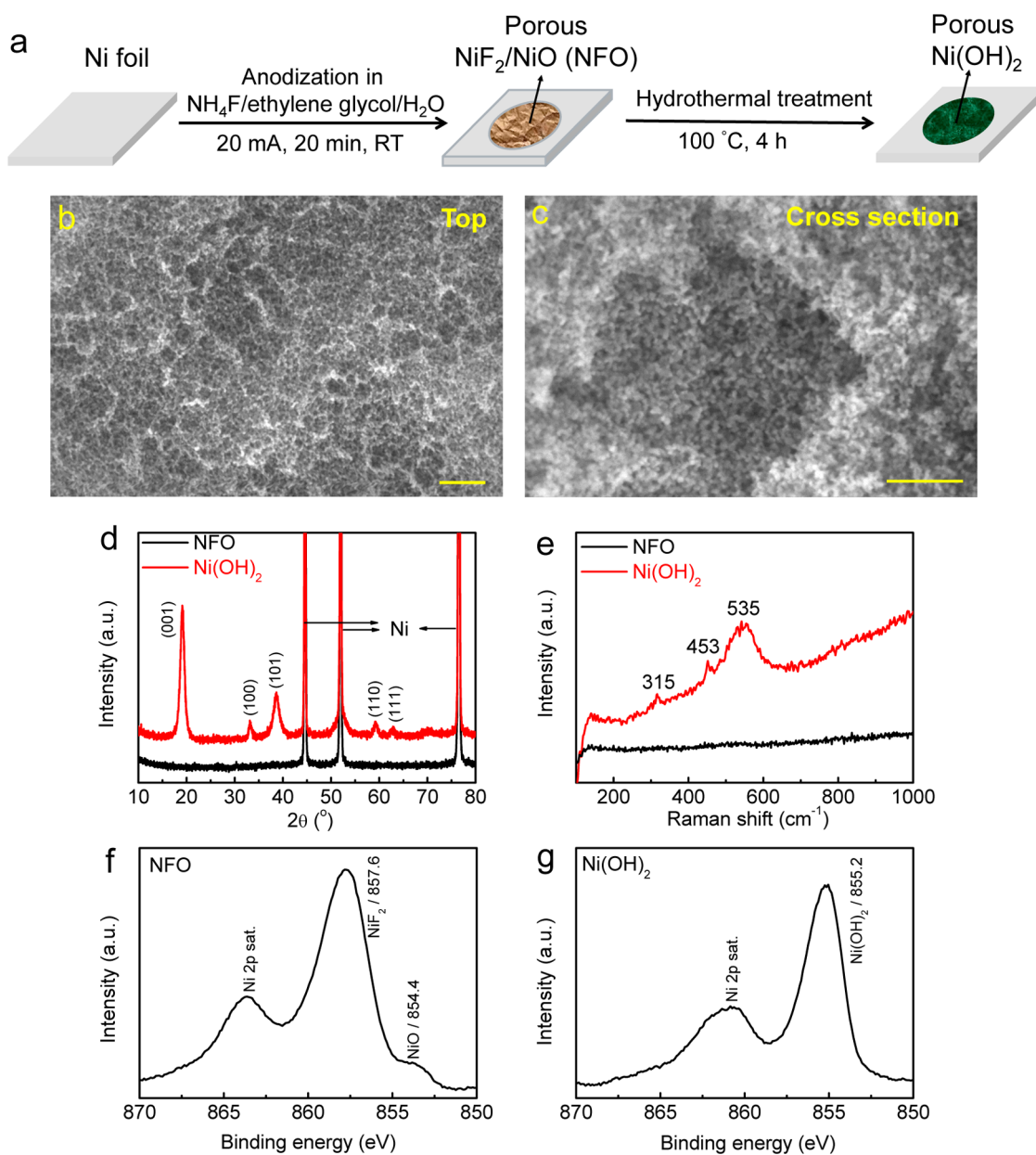
Figure 1. (a) Schematic for the fabrication process of the 3-D nanoporous Ni(OH)$_2$ thin-film. Anodization is done on a Ni-foil in the presence of NH$_4$F, followed by heating to 100 °C in an autoclave half-filled with aqueous NaOH (0.1 M). (b) Top and (c) magnified-cross sectional SEM images of the anodically formed nanoporous layer. The scale bar in (b,c) denotes 200 nm. (d) XRD patterns and (e) Raman spectra of the nickel fluoride/oxide nanoporous layers before (NFO, black line) and after (Ni(OH)$_2$, red line) hydrothermal treatment. (f,g) Ni 2p XPS spectra of the (f) NFO and (g) Ni(OH)$_2$.

supercapacitors. In this work, we report an approach to anodically grow a nickel fluoride/oxide thin-film with a 3-D nanoporous structure and to convert those films into 3-D nanoporous Ni(OH)$_2$ thin-films using hydrothermal treatment. The fabricated 3-D nanoporous Ni(OH)$_2$ thin-film delivers promising ECs performance in both three electrode testing and asymmetric two electrode supercapacitor devices.

RESULTS AND DISCUSSION

In the approach here (Figure 1a), electrochemical anodic treatments on nickel foils were used to form a 3-D nanoporous Ni-based thin-film. Microscopy analysis (Figure 1b,c and Supporting Information Figure S1) show that the as-prepared anodic thin-film has a 3-D nanoporous structure throughout the entire layer with a pore size of ∼10 nm. A thinner porous layer can, to some extent, reduce the electrode resistance and enhance the EC performances;[14−17] a thin-film with a thickness of 150−200 nm (Supporting Information Figure S1a) was fabricated and investigated in this work. After hydrothermal treatment, the 3-D nanoporous thin-film still maintains its porous morphology without observable damage or blocking of the nanopores (Supporting Information Figure S2).

The crystalline structure and chemical composition of the 3-D nanoporous thin-film were investigated by
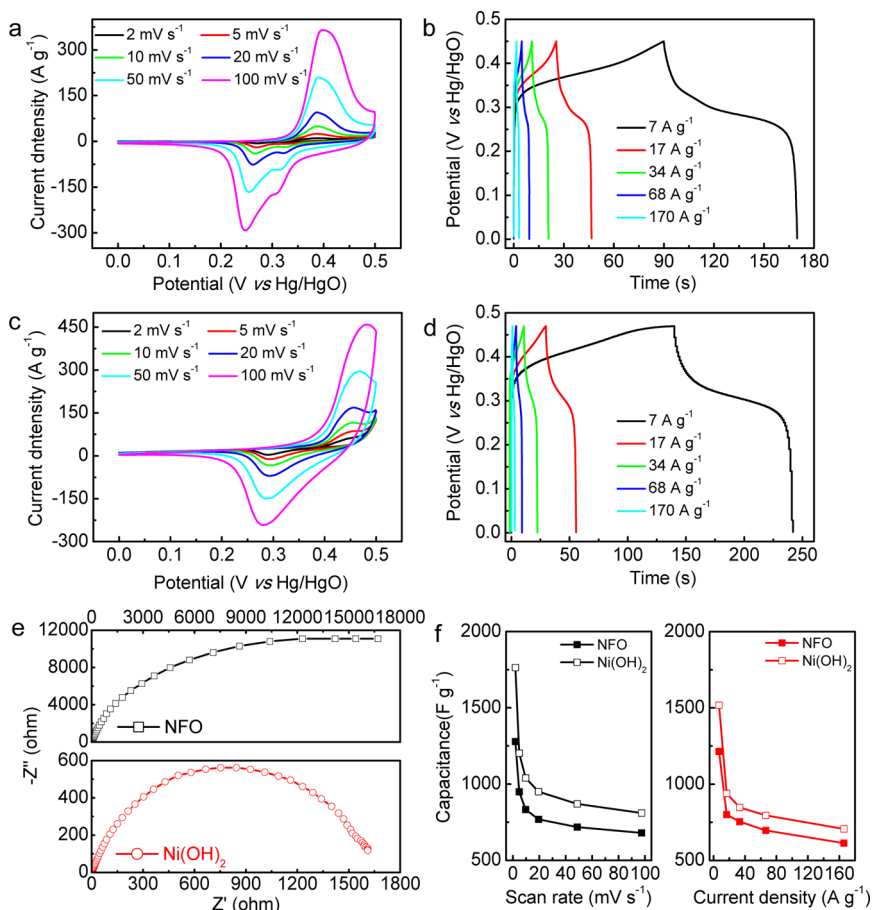
Figure 2. Electrochemical performance of the 3-D nanoporous NFO and Ni(OH)$_2$ thin-film electrodes tested in a three electrode cell. (a) Cyclic voltammograms (CVs) of the NFO performed at different scan rates. (b) Discharge/charge profiles of the NFO obtained at different current densities. (c) CVs of the Ni(OH)$_2$ performed at different scan rates. (d) Discharge/charge profiles of the Ni(OH)$_2$ obtained at different current densities. (e) Nyquist plots of the NFO (black) and Ni(OH)$_2$ (red) nanoporous electrodes. (f) Variation of the capacitance vs scan rates (black) and current densities (red).

X-ray diffraction (XRD, Figure 1d), Raman spectroscopy (Figure 1e), and X-ray photoelectron spectroscopy (XPS, Figure 1f,g and Supporting Information Figure S3). The anodically formed nanoporous thin-film shows an amorphous phase, which is composed of Ni, F, and O (nickel fluoride/oxide composite, NFO). The amorphous NFO was converted to highly crystalline Ni(OH)$_2$ (PDF #00-014-0117) after the hydrothermal treatment. From Raman analyses, typical bands for Ni(OH)$_2$ at 315, 453, and 535 cm^{-1} were identified after hydrothermal treatment.[18] The conversion from NFO to Ni(OH)$_2$ was also supported by fitting the XPS Ni 2p spectra (Figure 1f,g). The peak at 854.4 eV in Figure 1f is attributed to NiO,[19] while the peak at 857.6 eV is from NiF$_2$.[20] And the peak at 855.2 eV in the XPS spectrum of the hydrothermally treated sample is attributed to Ni(OH)$_2$.[21] The successful conversion from amorphous NFO to highly crystalline Ni(OH)$_2$ is based on the well-established in situ hydrothermal formation mechanism under high pressure/temperature atmosphere.[22] Possible reactions to form Ni(OH)$_2$ include NiF$_2$ + 2 NaOH → Ni(OH)$_2$ + 2 NaF.

To test the EC performances of the nanoporous NFO and Ni(OH)$_2$, three electrode testing (Figure 2) was performed in 6 M aq KOH electrolyte with Pt and Hg/HgO as counter and reference electrodes, respectively. From the cyclic voltammograms (CVs) of NFO (Figure 2a), the anodic peak at 0.39 V (vs Hg/HgO) and the cathodic peak at 0.27 V (vs Hg/HgO) can be assigned to the redox reaction: NiO + OH$^-$ ⇌ NiOOH + e$^-$.[23] Another cathodic peak at 0.33 V (vs Hg/HgO) is probably from NiF$_2$ in the nanoporous layer.[24] The capacitance of the NFO calculated from the CV at 2 mV s^{-1} is 1280 F g^{-1} (for the calculation details, see the Supporting Information). Galvanostatic discharge/charge (GDC, Figure 2b) curves of the NFO at different current densities from 7 to 170 A g^{-1} show deviation from the typical triangular shape of EDLCs that indicates the Faradaic characteristics of the charge storage. The shoulders in the GDC graphs at 0.4 V (vs Hg/HgO) during charging and 0.3 V (vs Hg/HgO) during discharging indicate the redox reactions which are consistent with the CVs. The capacitance of the NFO calculated from GDC curves at a current density of 7 A g^{-1} is 1215 F g^{-1}. From CVs of the Ni(OH)$_2$ nanoporous layer (Figure 2c), a pair of redox reaction peaks at 0.45 V (vs Hg/HgO) and 0.29 V (vs Hg/HgO) is evident, which
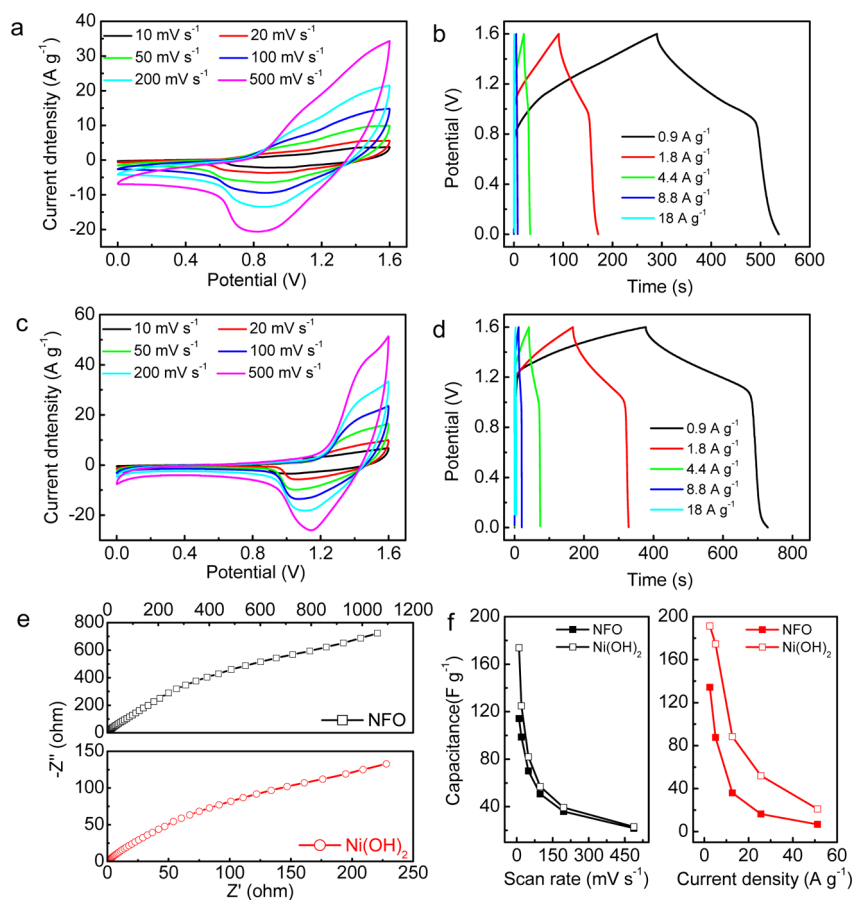
Figure 3. Electrochemical performance of the asymmetric supercapacitors based on the NFO and Ni(OH)$_2$ nanoporous electrodes. (a) CVs of the NFO performed at different scan rates. (b) Discharge/charge profiles of the NFO obtained at different current densities. (c) CVs of the Ni(OH)$_2$ performed at different scan rates. (d) Discharge/charge profiles of the Ni(OH)$_2$ obtained at different current densities. (e) Nyquist plots of the NFO (black) and Ni(OH)$_2$ (red) nanoporous electrodes. (f) Variation of the capacitance *vs* scan rates (black) and current densities (red).

represents the following redox reaction: Ni(OH)$_2$ + OH$^-$ ⇌ NiOOH + H$_2$O + e$^-$.[25] The capacitance of the Ni(OH)$_2$ calculated from the CV at 2 mV s^{-1} is 1765 F g^{-1}. Compared with the CVs of the NFO, the redox reaction peaks of the Ni(OH)$_2$ shift positively, which indicates a wider potential window can be anticipated without water electrolysis. The GDC curves of the Ni(OH)$_2$ show similar shape to the NFO but with a slightly elevated discharge/charge plateau, which is consistent with CVs. The capacitance of the Ni(OH)$_2$ calculated from GDC curves at a current density of 7 A g^{-1} is 1519 F g^{-1}. Further investigations on the EC performance of the 3-D nanoporous layers in three electrode cell were performed using electrochemical impedance spectroscopy (EIS). By simulating EIS data according to the equivalent circuit in Supporting Information Figure S4, the Nyquist plots of the nanoporous layers (Figure 2e) can be divided into two portions: (1) At high frequency, the intercept at the real axis represents the equivalent series resistance (R_{ESR}), which is a combination of ionic resistance of the electrolytes, electronic resistance of the electrode materials, and interface resistance. (2) The semicircle observed at the high-to-medium frequency region corresponds to the charge-transfer

resistance (R_{ct}), which is related to the Faradaic reactions and the electric double-layer capacitance (CPE$_{dl}$) at the electrode/electrolyte interfaces. For pseudocapacitors, R_{ESR} and R_{ct} are more informative because they reflect the electrical characteristics of the electrodes. Both nanoporous NFO and Ni(OH)$_2$ have low R_{ESR} on the same order of magnitude, 1.28 ± 0.02 and 3.13 ± 0.02 Ω, respectively, which indicates less internal resistance in the EC devices. Furthermore, R_{ct} for NFO and Ni(OH)$_2$ were calculated to be 28.56 ± 0.008 and 1.63 ± 0.006 kΩ, respectively. The greatly reduced R_{ct} in the nanoporous Ni(OH)$_2$ indicates its improved electrical conductivity and fast Faradaic/redox reactions after the hydrothermal treatment. The capacitance of the Ni(OH)$_2$ is enhanced at different discharge/charge rates (Figure 2f), which also indicates an improved ECs performance after hydrothermal treatment.

To access the practical supercapacitor device performance of the fabricated nanoporous layers, asymmetric two electrode cells were assembled using 6 M aq KOH as the electrolyte and porous activated carbon as the negative electrodes (see Experimental Section). The EC behavior of the samples was evaluated by calculating the specific capacitance of the entire device
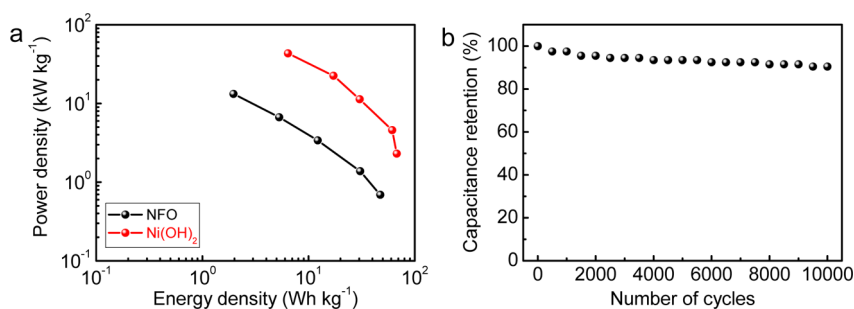
Figure 4. (a) Ragone plot of the nanoporous layers. (d) Capacitance retention of 10 000 charge/discharge cycles on the nanoporous Ni(OH)$_2$.

including both positive and negative electrodes from CVs and GDCs. Electrochemical characterizations were performed within a potential window between 0 and 1.6 V. From the CVs of NFO at different scan rates from 10 to 500 mV s^{-1} (Figure 3a), an anodic peak at 1.2 V and a cathodic peak at 1.0 V can be assigned to the redox reaction: NiO + OH$^-$ $\rightleftharpoons$ NiOOH + e$^-$.[26] The capacitance calculated from the CV at a scan rate of 10 mV s^{-1} is 114 F g^{-1}. GDC tests on the NFO were performed at current densities from 0.9 to 18 A g^{-1} (Figure 3b). The shoulders at 1.2 V during the charging and 1.0 V during the discharging indicate the redox reactions which are consistent with the CVs. The discharge capacitance at 0.9 A g^{-1} is calculated to be 135 F g^{-1}. After hydrothermal treatment to Ni(OH)$_2$, the measured CVs (Figure 3c) and GDC curves (Figure 3d) of the nanoporous Ni(OH)$_2$ show positively shifted redox reactions compared with NFO. Redox reactions occurred at 1.4 V (anodic) and 1.1 V (cathodic) representing: Ni(OH)$_2$ + OH$^-$ $\rightleftharpoons$ NiOOH + H$_2$O + e$^-$.[27] Furthermore, the capacitance of the Ni(OH)$_2$ calculated from the CV at 10 mV s^{-1} and GDC curve at 0.9 A g^{-1} is 174 and 192 F g^{-1}, respectively. To have a better understanding of the EC performances of the nanoporous layers, EIS was also performed on the asymmetric supercapacitor devices (Figure 3e). In the supercapacitor devices based on both nanoporous NFO and Ni(OH)$_2$, low $R_{ESR} \sim 0.64 \pm 0.03$ and 0.57 ± 0.04 Ω, respectively, are obtained. Furthermore, R_{ct} values for NFO and Ni(OH)$_2$ were calculated to be 833.5 ± 0.6 and 175.9 ± 0.4 Ω, respectively. It is gratifying that even after assembly into asymmetric supercapacitors, the Ni(OH)$_2$ still has greatly reduced resistance when compared with NFO. Furthermore, at different discharge/charge rates (Figure 3f), Ni(OH)$_2$ also delivers enhanced EC performance after hydrothermal treatment.

The advanced ECs performance of the fabricated devices that use the nanoporous NFO and Ni(OH)$_2$ as electrodes are also reflected by their energy and power densities, as shown in the Ragone plot (Figure 4a). The maximum energy density (E_{max}) and power density (P_{max}) of the nanoporous NFO were calculated to be 48 Wh kg^{-1} and 14 kW kg^{-1}, respectively; the nanoporous Ni(OH)$_2$ gave values for E_{max} of 68 Wh kg^{-1} and P_{max} of 44 kW kg^{-1}. Considering the capacitance of NFO and Ni(OH)$_2$ obtained both in three electrode and two electrode testing, the fabricated nanoporous layers deliver superior EC performances compared to carbonaceous materials and most other state-of-the-art nanostructured supercapacitors based on NiO and Ni(OH)$_2$ (Supporting Information Table S1).[28] Moreover, the devices were tested at 18 A g^{-1} for cyclability by running them through 10 000 discharge/charge cycles. More than 90% retention was obtained (Figure 4b) without obvious change in the 3-D nanoporous structure of Ni(OH)$_2$ after testing (Supporting Information Figure S5). These results suggest the utility of these devices in practical EC applications. The 3-D open channel in the nanoporous structure, with its high resulting surface area, provides more electrochemically active sites for redox reactions and fast ion transport. These attributes contribute to the obtained high capacitances.

CONCLUSION

In summary, a 3-D nanoporous nickel fluoride/oxide thin-film was anodically fabricated and hydrothermally treated to form a highly crystalline Ni(OH)$_2$ nanoporous layer. The nanoporous Ni(OH)$_2$ thin-film on nickel foils can be directly used as additive-free electrode supercapacitors. The Ni(OH)$_2$ nanoporous layer delivers a high capacitance of $\sim$1765 F g^{-1}. When assembled into asymmetric capacitor devices with porous activated carbon as the negative electrode, the entire device provides a capacitance of $\sim$192 F g^{-1} with energy and power density of $\sim$68 Wh kg^{-1} and 44 kW kg^{-1}, respectively, which is superior to those of other nanostructured Ni(OH)$_2$, thus providing a promising material for supercapacitors.

EXPERIMENTAL SECTION

Fabrication. Nickel foils (0.125 mm, 99.9%, Sigma-Aldrich) were sonicated in ethanol for 1 h before being used as

substrates. Nanoporous nickel fluoride/oxide thin-films were anodically grown in a solution of 0.2 M NH$_4$F ($\geq$98%, Sigma-Aldrich) with 2 M deionized water in ethylene glycol (Fisher Scientific) at constant current of 20 mA for 20 min in a two

electrode setup at room temperature. After anodization, the samples were rinsed with H_2O followed by drying under nitrogen gas flow. Hydrothermal treatments on the as-prepared 3-D nanoporous nickel fluoride/oxide thin-film were conducted in an aqueous solution of 0.1 M NaOH at 100 °C for 4 h to form highly crystalline $Ni(OH)_2$. The autoclave (Parr Instrument Company, model 4744, 45 mL capacity) was filled to ~50% volume capacity with 0.1 M NaOH during the hydrothermal treatment. *Caution! Never fill an autoclave to more than 50%.* Afterward, the samples were washed several times with H_2O and dried under nitrogen gas flow. The mass loading of the NFO and $Ni(OH)_2$ films are approximately 0.06 and 0.04 mg cm^{-2}, respectively.

Characterization. A JEOL 6500F scanning electron microscope (SEM) was used to investigate the morphology of the samples. The crystal structure of the thin-film was evaluated using X-ray diffraction (XRD) analysis on a Rigaku D/Max Ultima II (Rigaku Corporation, Japan) configured with Cu Kα radiation, graphite monochromator, and scintillation counter. Raman spectra were recorded with a Renishaw Raman RE01 scope (Renishaw Inc.) using a 514 nm excitation argon laser. Investigation of the chemical composition of the nanoporous layers was performed using X-ray photoelectron spectroscopy (PHI Quantera XPS, Physical Electronics). An Al anode at 25 W was used as the X-ray source with a pass energy of 26.00 eV, 45° take off angle, and 100 μm beam size. A pass energy of 140 eV was used for survey spectra, and 26 eV for atomic concentration spectra.

Electrochemical Measurements. The nanoporous layers on nickel foils were directly used as additive-free electrodes (without binder, additional current collector or conducting carbon). Three electrode testing was performed in 6 M aq KOH using Pt foil and Hg/HgO as the counter and reference electrodes, respectively. The CVs were measured at different scan rates from 2 to 100 mV s^{-1} in a potential window from 0 to 0.5 V (vs Hg/HgO). The galvanostatic discharge/charge curves were recorded at different current densities from 7 to 170 A g^{-1}. For the two electrode testing, the samples were assembled in an asymmetric cell with porous activated carbon film (mixed with 10% PTFE) as the negative electrode and glass microfiber filters (Whatman GF/F) as separators immersed in 6 M aq KOH. The mass ratio between the positive and negative electrodes is estimated according to the charge balance: $q_+ = q_-$. The CVs were measured at different scan rates from 10 mV s^{-1} to 500 mV s^{-1} in a potential window from 0 to 1.6 V. The galvanostatic discharge/charge curves were recorded at different current densities from 0.9 to 18 A g^{-1} (based on total mass of the two electrodes). And the EIS were carried out on the fresh cells at open circuit potentials with a frequency range from 10^{-2} to 1×10^5 Hz with ac signal amplitude of 5 mV. The CVs, galvanostatic discharge/charge curves and EIS measurements were carried out with an electrochemical analyzer (CHI 608D, CH Instruments, USA). The discharge/charge cycling tests were performed on a multichannel battery analyzer (BST8-WA, MTI Corporation, USA).

Conflict of Interest: The authors declare no competing financial interest.

Supporting Information Available: Calculations, additional figures and table. This material is available free of charge *via* the Internet at http://pubs.acs.org.

REFERENCES AND NOTES

1. Pech, D.; Brunet, M.; Durou, H.; Huang, P.; Mochalin, V.; Gogotsi, Y.; Taberna, P.-L.; Simon, P. Ultrahigh-Power Micrometre-Sized Supercapacitors Based on Onion-Like Carbon. *Nat. Nanotechnol.* **2010**, *5*, 651–654.

2. Lang, X.; Hirata, A.; Fujita, T.; Chen, M. Nanoporous Metal/Oxide Hybrid Electrodes for Electrochemical Supercapacitors. *Nat. Nanotechnol.* **2011**, *6*, 232–236.

3. Zhu, Y.; Murali, S.; Stoller, M. D.; Ganesh, K. J.; Cai, W.; Ferreira, P. J.; Pirkle, A.; Wallace, R. M.; Cychosz, K. A.; Thommes, M.; *et al.* Carbon-Based Supercapacitors Produced by Activation of Graphene. *Science* **2011**, *332*, 1537–1541.

4. Kötz, R.; Carlen, M. Principles and Applications of Electrochemical Capacitors. *Electrochim. Acta* **2000**, *45*, 2483–2498.

5. Conway, B. E. Transition from "Supercapacitor" to "Battery" Behavior in Electrochemical Energy Storage. *J. Electrochem. Soc.* **1991**, *138*, 1539–1548.

6. Wang, G.; Zhang, L.; Zhang, J. A Review of Electrode Materials for Electrochemical Supercapacitors. *Chem. Soc. Rev.* **2012**, *41*, 797–828.

7. Zhang, L. L.; Zhao, X. S. Carbon-Based Materials as Supercapacitor Electrodes. *Chem. Soc. Rev.* **2009**, *38*, 2520–2531.

8. Armand, M.; Endres, F.; MacFarlane, D. R.; Ohno, H.; Scrosati, B. Ionic-Liquid Materials for the Electrochemical Challenges of the Future. *Nat. Mater.* **2009**, *8*, 621–629.

9. Fan, Z.; Yan, J.; Wei, T.; Zhi, L.; Ning, G.; Li, T.; Wei, F. Asymmetric Supercapacitors Based on Graphene/MnO_2 and Activated Carbon Nanofiber Electrodes with High Power and Energy Density. *Adv. Funct. Mater.* **2011**, *21*, 2366–2375.

10. Aricò, A. S.; Bruce, P.; Scrosati, B.; Tarascon, J.-M.; Schalkwijk, W. Nanostructured Materials for Advanced Energy Conversion and Storage Devices. *Nat. Mater.* **2005**, *4*, 366–377.

11. Yuan, C.; Zhang, X.; Su, L.; Gao, B.; Shen, L. Facile Synthesis and Self-Assembly of Hierarchical Porous NiO Nano/Micro Spherical Superstructures for High Performance Supercapacitors. *J. Mater. Chem.* **2009**, *19*, 5772–5777.

12. Wang, H.; Casalongue, H. S.; Liang, Y.; Dai, H. $Ni(OH)_2$ Nanoplates Grown on Graphene as Advanced Electrochemical Pseudocapacitor Materials. *J. Am. Chem. Soc.* **2010**, *132*, 7472–7477.

13. Hou, Y.; Cheng, Y.; Hobson, T.; Liu, J. Design and Synthesis of Hierarchical MnO_2 Nanospheres/Carbon Nanotubes/Conducting Polymer Ternary Composite for High Performance Electrochemical Electrodes. *Nano Lett.* **2010**, *10*, 2727–2733.

14. Yuan, C.; Li, J.; Hou, L.; Zhang, X.; Shen, L.; Lou, X. W. Ultrathin Mesoporous $NiCo_2O_4$ Nanosheets Supported on Ni Foam as Advanced Electrodes for Supercapacitors. *Adv. Funct. Mater.* **2012**, *22*, 4592–4597.

15. Guan, C.; Liu, J.; Cheng, C.; Li, H.; Li, X.; Zhou, W.; Zhang, H.; Fan, H. J. Hybrid Structure of Cobalt Monoxide Nanowire@Nickel Hydroxidenitrate Nanoflake Aligned on Nickel Foam for High-rate Supercapacitor. *Energy Environ. Sci.* **2011**, *4*, 4496–4499.

16. Wang, Y. L.; Zhao, Y. Q.; Xu, C. L.; May, J. 3D Nickel Foam Electrode Be the Promising Choice for Supercapacitors? *Solid State Electrochem.* **2012**, *16*, 829–834.

17. Huang, J.; Zhu, J.; Cheng, K.; Xu, Y.; Cao, D.; Wang, G. Preparation of Co_3O_4 Nanowires Grown on Nickel Foam with Superior Electrochemical Capacitance. *Electrochim. Acta* **2012**, *75*, 273–278.

18. Li, H. B.; Yu, M. H.; Wang, F. X.; Liu, P.; Liang, Y.; Xiao, J.; Wang, C. X.; Tong, Y. X.; Yang, G. W. Amorphous Nickel Hydroxide Nanospheres with Ultrahigh Capacitance and Energy Density as Electrochemical Pseudocapacitor Materials. *Nat. Commun.* **2013**, *4*, 1894.

19. Carley, A. F.; Jackson, S. D.; Roberts, M. W.; O'Shea, J. Alkali Metal Reactions with Ni(110)-O and NiO(100) surfaces. *Surf. Sci.* **2000**, *454–456*, 141–146.

20. Ureta-Zañartu, M. S.; Berríos, C.; Pavez, J.; Zagal, J.; Gutiérrez, C.; Marco, J. F. Electrooxidation of 2-Chlorophenol on PolyNiTSPc-Modified Glassy Carbon Electrodes. *J. Electroanal. Chem.* **2003**, *553*, 147–156.

21. Alammar, T.; Shekhah, O.; Wohlgemuth, J.; Mudring, A.-V. Ultrasound-Assisted Synthesis of Mesoporous β-$Ni(OH)_2$ and NiO Nano-Sheets Using Ionic Liquids. *J. Mater. Chem.* **2012**, *22*, 18252–18260.

22. Yang, Y.; Wang, X.; Zhong, C.; Sun, C.; Li, L. Ferroelectric $PbTiO_3$ Nanotube Arrays Synthesized by Hydrothermal Method. *Appl. Phys. Lett.* **2008**, *92*, 122907.

23. Xia, X.; Tu, J.; Mai, Y.; Chen, R.; Wang, X.; Gu, C.; Zhao, X. Graphene Sheet/Porous NiO Hybrid Film for Supercapacitor Applications. *Chem.—Eur. J.* **2011**, *17*, 10898–10905.

24. Yang, Y.; Ruan, G.; Xiang, C.; Wang, G.; Tour, J. M. Flexible Three-Dimensional Nanoporous Metal-Based Energy Devices. *J. Am. Chem. Soc.* **2014**, *136*, 6187–6190.

25. Zhang, H.; Zhang, X.; Zhang, D.; Sun, X.; Lin, H.; Wang, C.; Ma, Y. One-Step Electrophoretic Deposition of Reduced Graphene Oxide and Ni(OH)$_2$ Composite Films for Controlled Syntheses Supercapacitor Electrodes. *J. Phys. Chem. B* **2013**, *117*, 1616–1627.

26. Lee, J. W.; Ahn, T.; Kim, J. H.; Ko, J. M.; Kim, J.-D. Nanosheets Based Mesoporous NiO Microspherical Structures *via* Facile and Template-Free Method for High Performance Supercapacitors. *Electrochim. Acta* **2011**, *56*, 4849–4857.

27. Cao, L.; Kong, L.-B.; Liang, Y.-Y.; Li, H.-L. Preparation of Novel Nano-Composite Ni(OH)$_2$/USY Material and Its Application for Electrochemical Capacitance Storage. *Chem. Commun.* **2004**, 1646–1647.

28. Wang, Q.; Wang, X.; Liu, B.; Yu, G.; Hou, X.; Chen, D.; Shen, G. NiCo$_2$O$_4$ Nanowire Arrays Supported on Ni Foam for High-Performance Flexible All-Solid-State Supercapacitors. *J. Mater. Chem. A* **2013**, *1*, 2468–2473.